Desalination and Water Treatment
www.deswater.com
doi: 10.5004/dwt.2020.25732

192 (2020) 44–53
July

Numerical simulation on horizontal tube falling film column flow with influence of gas crossflow

Xueshuo Chen[a], Tao Lu[a], Jie Wang[a], Xue Chen[a,*], Shengqiang Shen[b], Jiang Sheng[c], Xuan Chen[c]

[a]*School of Mechanical and Electrical, Beijing University of Chemical Technology, Beijing 100029, China, email: xchen@buct.edu.cn (X. Chen)*
[b]*School of Energy and Power Engineering, Dalian University of Technology, Dalian 116024, China*
[c]*Science and Technology on Space Physics Laboratory, Beijing 100076, China*

Received 11 September 2019; Accepted 22 February 2020

ABSTRACT

Gas crossflow changes the flow behavior, which leads to an influence on the system efficiency, especially in larger evaporators. A three-dimensional numerical simulation was performed to investigate the flow characteristics of horizontal tube falling film with gas crossflow using volume of fluid method. The deflection of the liquid column and film thickness distribution involving the effects of spray Reynolds number and gas velocity were analyzed. The results show the three-dimensional film thickness distribution around a horizontal tube. The deflection angle of the liquid column increases with the increasing of crossflow velocity and decreasing of spray Reynolds number. The liquid film in the windward side is thinner than that in the leeward side and the film with minimum thickness appears at ϕ = 75°–150° in "stable region." Furthermore, the enhancement in spray Reynolds number obviously promotes film thickness in the leeward side, but the enhancement in crossflow velocity thins the film thickness, especially in the windward side.

Keywords: Horizontal tube falling film; Column flow; Film thickness; Gas crossflow

1. Introduction

Horizontal tube falling film evaporation is the core technology in low temperature multi-effect evaporation desalination due to high heat transfer rate, low temperature difference, and good anti-scale performance [1–4]. The flow state of liquid film around the horizontal tube directly dominates the heat transfer and influences the system [5–8], therefore, numerous studies have been performed to investigate the liquid film flow characteristics.

Xu et al. [9] investigated the film thickness at the circumferential angle of 45°, 90°, and 135° involving the effects of tube diameter and spray density with capacitance method. Rogers and Goindi [10], Narváez-Romo and Simões-Moreira [11], and Hou et al. [12] measured the film thickness around the horizontal tube falling film by conductivity method. Hou et al. [12] pointed out that the minimal film location is in the range of 90°–115°. Gstoehl et al. [13] investigated the film thickness of horizontal tube falling film with Planar laser-induced fluorescence technology focusing on sheet flow, they found that the experimental result matches well with Nusselt theoretical value on the top perimeter, but is significantly smaller on the lower half tube. With a similar method, Chen et al. [14] captured the gas–liquid interface of column flow and presented the film thickness variation along the axial length and circumferential angle.

With the development of computational fluid dynamics, many scholars performed numerical simulations to investigate horizontal tube falling film with the volume of fluid method. Luo et al. [15], Zhao et al. [16], and Ji et al. [17] investigated the horizontal tube falling film flow with 2D models, their results on the location with minimal film

* Corresponding author.

thickness were inconsistent (125°, 110°–150°, and 120°, respectively). Killion and Garimella [18] firstly conducted a 3D simulation focusing on droplet flow and accurately obtained the flow behavior. Zhou et al. [19] stated that minimum film thickness approximately appears at the circumferential angle of 100°–140° and moves to the bottom with the spray density increasing. Li et al. [20] found that the thinnest film ranges in circumferential angle of 90°–100° for droplet flow and column flow and locates at about 120° for sheet flow. Hosseinnia et al. [21] demonstrated that the film thickness distribution at $l^* = 0$ agrees well with Nusselt's solution. Wang et al. [22] obtained the 3D thickness distributions with effects of Reynolds number and tube spacing in a quiescent surrounding, and pointed out the location of thinnest film.

In the large-scale evaporator, such as low temperature multi-effect distillation (LT-MED) desalination plant, gas crossflow is inevitable due to the vapor outlet location and tube arrangement, so that the gas flow redistributes the liquid film [3], as shown in Fig. 1. With the more studies went into the technology of horizontal tube falling film evaporation, it found that this disturbance largely influences the heat transfer efficiency through changing the film flow [23–25], which stimulates the scholars to further study the film state variation with the effects of gas flow.

The gas flow types in the horizontal tube bundle were classified into: concurrent (downward), counter-current (upward), and cross (sideward) vapor streams [1]. Yung et al. [26] found that liquid deflection and incomplete wetting would appear in the evaporation process with the vapor cross-flow. Hu and Jacobi [27] experimentally investigated the horizontal tube falling film in concurrent air flow and found the increment in transition Reynolds number from droplet flow to column flow in concurrent air flow. Lei et al. [28] studied the liquid column deflection in air crossflow and summarized a correction on deflection distance, they pointed out the deflection length of liquid column increases with the gas velocity. Li et al. [20] investigated the hydrodynamic characteristics of falling film with counter-current gas over horizontal tubes using a three-dimensional model. The simulation results of flow pattern agreed well with experiment results. With the increasing of counter-current gas flow velocity, the location of the thinnest film around the tube rises and the film thickness thickens. Ruan et al. [29] performed an experimental study on the effects of the counter-current gas flow on falling film pattern transitions.

Based on the above review, we found that the open literatures on horizontal tube falling film flow with gas crossflow is limited. Therefore, this study is aimed at obtaining the liquid column deflection and film thickness distribution of horizontal tube falling film in gas crossflow involving the effects of film Reynolds number and gas flow velocity.

2. Numerical simulation approach

2.1. Physical model and mesh strategy

As shown in Fig. 2a, two horizontal tubes with slot inlet has been applied in this simulation in order to obtain accurate simulation results, which helps to obtain the stable flow in the column flow Re range [30]. The fluid comes out from the slot inlet with size of $l_x \times w$ and then spreads around the upper tube (namely distribution tube), then falls onto the lower tube as column flow with typical Reynolds number. The gas flow generates from one side surface defined as velocity inlet and sweeps through the tubes, while the opposite side surface is pressure outlet. The parameters of this model and the properties of fluids are listed in Tables 1 and 2, respectively.

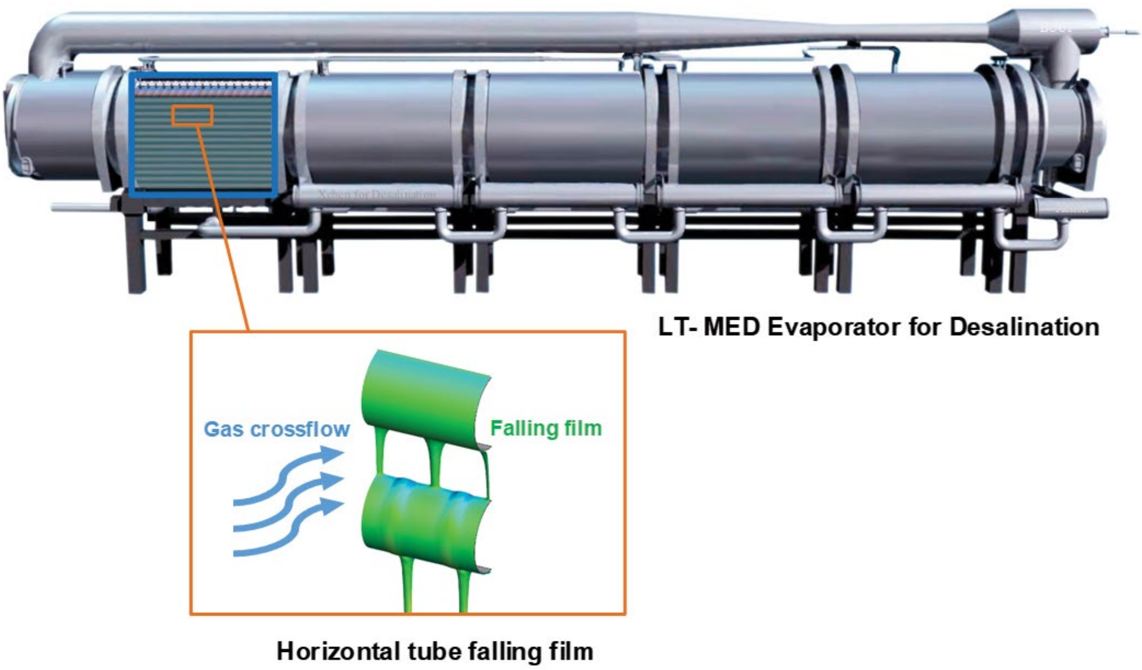

Fig. 1. Schematic of LT-MED desalination with horizontal tube falling film.

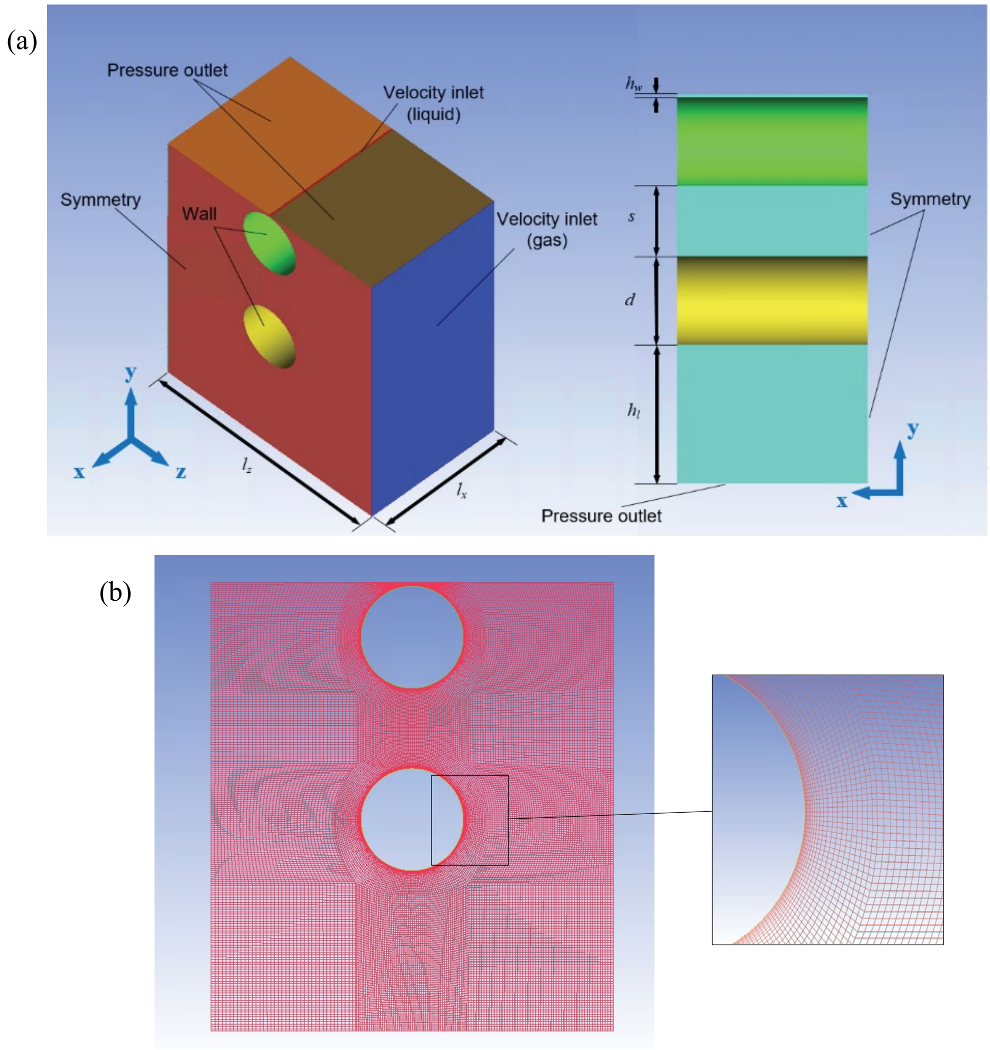

Fig. 2. (a and b) Dominant region and grid.

2.2. Mathematical model

The detailed description of this model was given in [24].

2.3. Simulation setup and grid independence

All the simulations in this study were performed by the ANSYS Fluent 16.0 [31]. The same setups with [24] were adopted in this simulation.

The grid independence verification was performed by tracing the film thickness at four typical circumferential angles of –120°, –60°, 60°, and 120°. The film thickness around the lower tube in time-average (from t = 2.3 to 2.4 s with interval of 0.005 s) with the element number of 3,174,200; 3,654,180; and 3,978,188 under the condition of d = 25.4 mm and s = 20 mm are shown in Fig. 3. It was found that the maximum difference in film thickness between grid of 3,654,180 and 3,978,188 elements was below 4%. Hence, a grid of 3,654,180 cells with a minimum cell length of 0.02 mm and a maximum length of 0.4 mm was adopted in the following simulations.

3. Results and discussion

The film thickness distribution along circumferential tube surface can be divided into two parts: windward side (ϕ = 0°–180° clockwise) and leeward side (ϕ = 0° to –180° anticlockwise). The gas crossflow significantly affects the liquid film of windward side around distribution tube and drives the departure point toward leeward side, which produces a slight deflection. Consequently, with the drag force of gas crossflow, the liquid column between the tubes continues to deviate from the central line. The dimensionless length l^* is defined as follows [14]:

$$l^* = \frac{l}{\lambda} \tag{1}$$

where l refers to the distance from liquid column centerline to the target location in a flow element and λ refers to the spacing between two centerlines of adjacent liquid columns, as shown in Figs. 4b and c.

Table 1
Parameters of numerical simulation

Physical parameters	Range
d	25.4 mm
h_w	1 mm
h_l	40 mm
Re	221, 258, 295
l_x	60 mm
l_z	100 mm
s	20 mm
w	0.73 mm
u	0.2, 0.6, 1 m/s
θ	10°

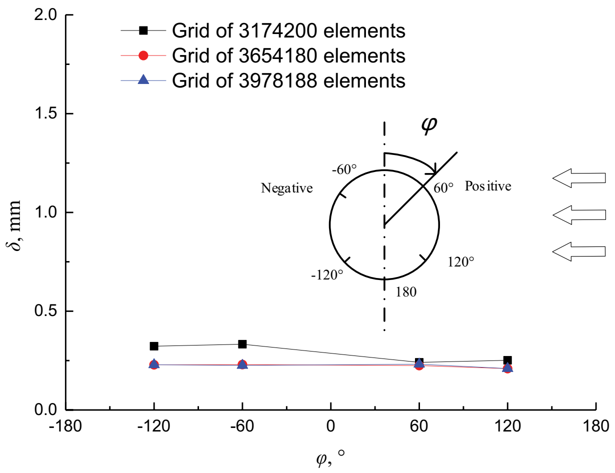

Fig. 3. Grid independence.

The formation progress of the horizontal tube falling film under gas crossflow can help us to further understand the mechanism. The appendix videos illustrate the whole distributing including liquid film spreading, impinging and converging, it can be found that the departure points on distribution tube generate at leeside, which forms a slight film deflection angle β_f, as shown in Fig. 4a. The liquid columns stabilize after they touch the lower tube with a column deflection angle β_c, as shown in Fig. 4a. The liquid film spreads toward both leeward and windward, then accumulates at the windward side and departures.

3.1. Liquid column deflection

Due to the gas crossflow, that the liquid accumulation at bottom of upper tube deflects marginally toward leeward results in a deflection angle β_f, while the liquid column forms a deflection angle β_c, as shown in Fig. 4a. However, indeed, the value of β_f is small in this crossflow range, hence we only focus on β_c which refers to the relationship between drag force and gravity for the liquid column in this study.

Yung et al. [26] simplified the liquid column and analyzed the forces balance, the relationship between gravity and crossflow drag force is:

$$\sin\beta_c = \frac{F_d}{G} \tag{2}$$

where F_d is the drag force and can be calculated by the following equation:

$$F_d = \frac{1}{2} C_d L d^* \rho_{\text{gas}} \left(u_{\text{gas}} \cos\alpha\right)^2 \tag{3}$$

According to Yung's analysis, the liquid column is simplified as a cylinder with a consist diameter d^*,

$$d^* = \left(\frac{16\lambda\Gamma}{\pi\rho_{\text{liquid}}}\right)^{0.5} \left(2gs\right)^{-0.25} \tag{4}$$

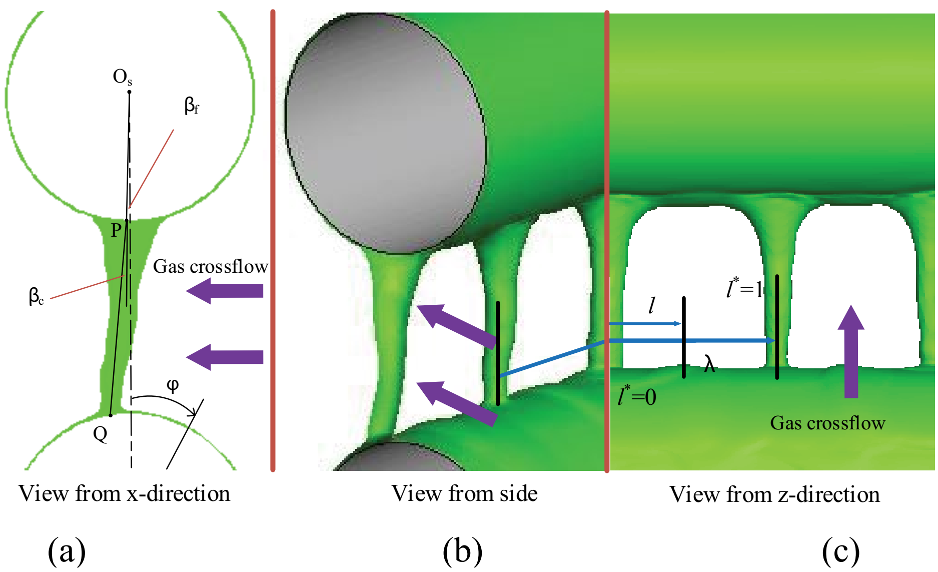

Fig. 4. Horizontal tube falling film with gas crossflow. View from (a) x-direction, (b) side, and (c) z-direction.

where λ refers to the instability wave length defined as:

$$\lambda = 2\pi\sqrt{\frac{n\sigma}{\rho_1 g}} \quad (5)$$

as for deflection angle β_c, the theoretical values calculated by Yung's relationship and the simulated results are presented in Figs. 5a and b, they show the same tendency with crossflow velocity and spray Reynolds number. With increasing of crossflow velocity, the β_c increases obviously due to the enhancement of F_d, but the simulated values are larger than the theoretical value. That may be caused by the two following reasons: one is the difference in crossflow velocities that results from an idealized theoretical model. In fact, the crossflow accelerates when it goes through the intertube gap, as shown in Fig. 5c. The other reason is the different initial departure velocities of liquid column in z-direction.

As we know from Eqs. (3) and (4), the F_d is proportional to $Re^{0.5}$, while the G is proportional to Re, hence, with the Re increases, the β_c decreases. Fig. 5b shows that the theoretical values are generally smaller than that simulated and the gap narrows with the Re increasing, that because larger Re leads to a more symmetrical film distribution for an upper tube, the initial departure velocity in z-direction for the liquid column is closer to zero, which reduce the difference with the theoretical value.

3.2. Film thickness distribution

The film thickness distributions at three typical sections of l^* = 0, 0.25, and 0.5 (namely impingement section, transition section, and departure section) have been selected in this study. The whole film thickness along both sides has been taken into consideration due to the asymmetry resulted from gas crossflow, which is different from falling film in a quiescent environment [22].

3.2.1. Effect of gas crossflow velocity

Figs. 6a–c illustrates that the film thickness distribution under crossflow at l^* = 0, 0.25, and 0.5 with Re = 258.

As shown in Fig. 6a, generally, similar to the film thickness distribution in the quiescent environment [22], the film thickness with crossflow at the impingement section also decreases first after impingement and then increases when closes to bottom at both leeward and windward.

Table 2
Physical properties of fluids

Physical parameters	σ, N/m	μ, kg/(m s)	ρ, kg/m^3
Air	–	1.7894×10^{-5}	1.225
Water	0.072	1.003×10^{-3}	998.2

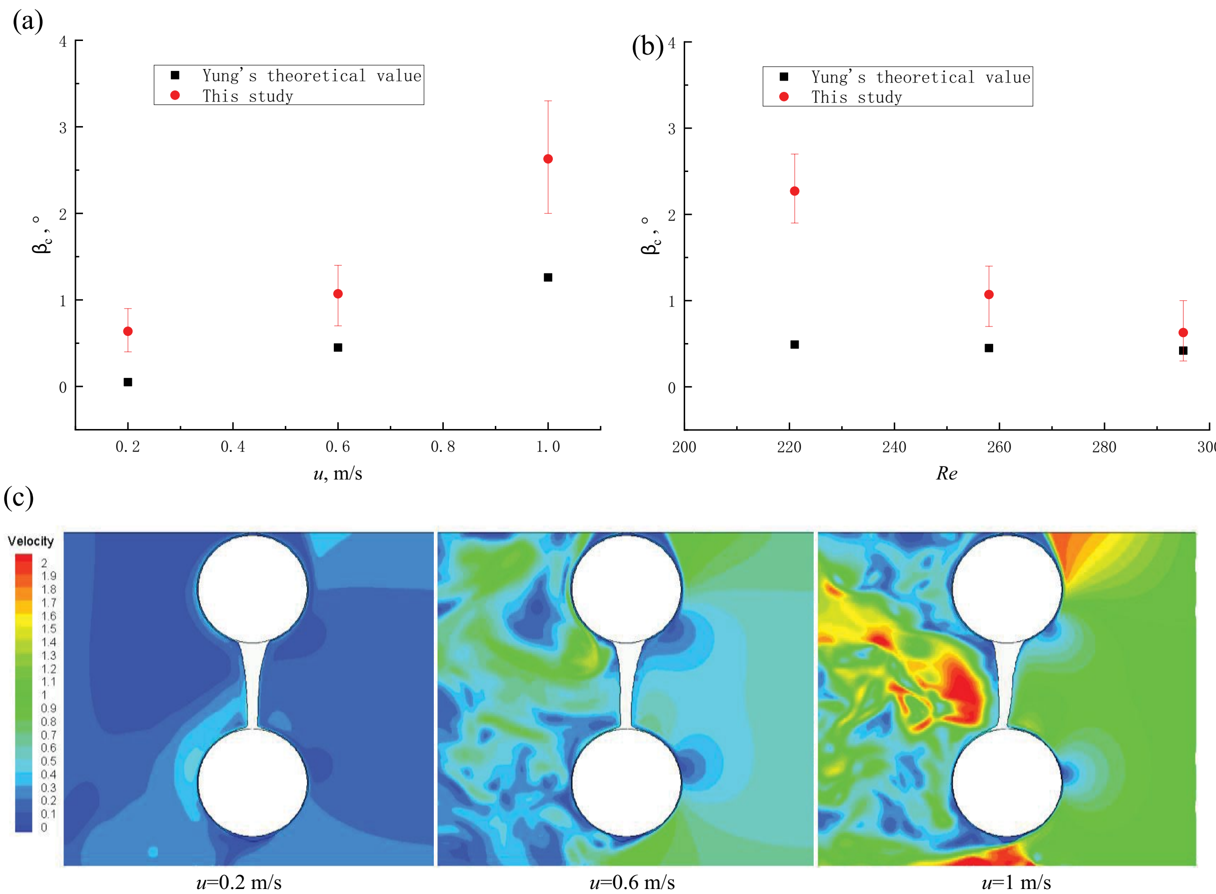

Fig. 5. Liquid column deflection. (a) β_c with u, (b) β_c with Re, and (c) velocity contours for Re = 258 at l^* = 0.

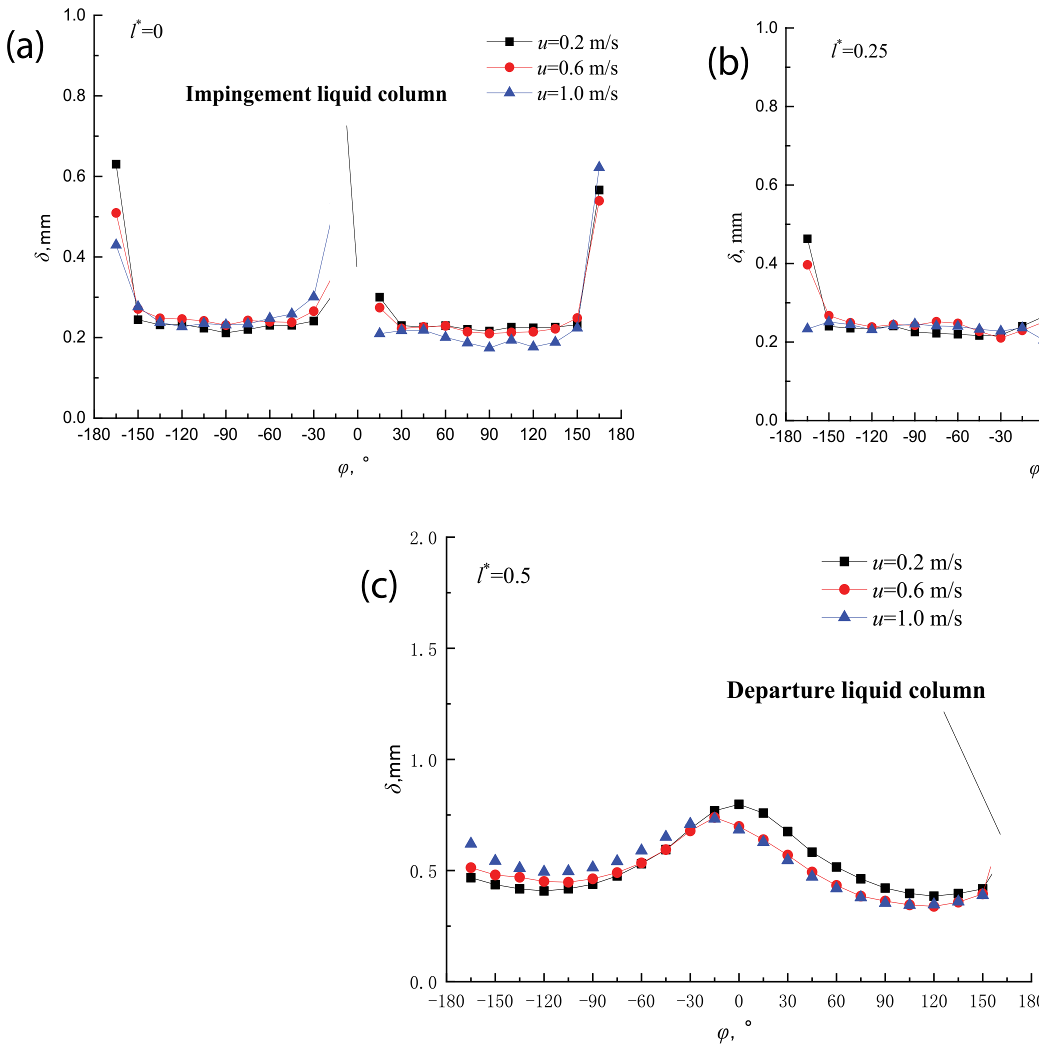

Fig. 6. Effect of gas crossflow velocity on time-average film thickness. (a) l^* = 0, (b) l^* = 0.25, and (c) l^* = 0.5.

However, it also shows the liquid column gradually moves to the leeside with the increasing of crossflow velocity. Moreover, the crossflow also reduces the film thickness at windward and increases that at leeward. Although the film thicknesses in the range from –45° to –150° and 30° to 150° are relatively uniform with the variation below ±15% of each average values, the gap in film thickness between two sides increases slightly with the gas flow velocity increasing.

As shown in Fig. 6b, the effect of crossflow velocity on film thickness is marginal, the film thickness at the transition section are uniform (0.2–0.25 mm) in the range from –150° to 150°. It also can be found that the liquid accumulation at the bottom slightly deflects to windward when the crossflow velocity reaches 1.0 m/s.

The curves in Fig. 6c shows the film thickness at departure section, the liquid forms a pump due to the convergence from two adjacent columns. It clearly illustrates that the crossflow intensifies the asymmetry of film thickness distribution. With respect to each liquid column centerline, the film thickness of u = 0.2 m/s at leeward is only 3.7% larger than windward in average, while that of u = 1 m/s at leeward is 25.3% larger than windward.

The three-dimensional morphology for film thickness which is supposed to be stripped from the tube is shown in Fig. 7. The distribution with u = 0.2 m/s is similar to that in the quiescent environment [22], but with the crossflow velocity increases, the film thickness in stable region decreases, the liquid pump in crest region moves to the leeward and the bottom region generally transfers to the windward. The above phenomenon mainly caused by two reasons: column deflection and the gas drag. The liquid column deflection results in the longer falling distance and the side impingement, which makes the film in leeward has a larger velocity.

Obviously, the thinnest film spreads over the area of l^* = 0–0.2 at ϕ = 75°–135° in a stable region of windward. The liquid column deflection also makes the nonuniform apportion and the gas near the interface in windward also promotes the velocity of the liquid film in some extant, which both cause the film thickness in a stable region further

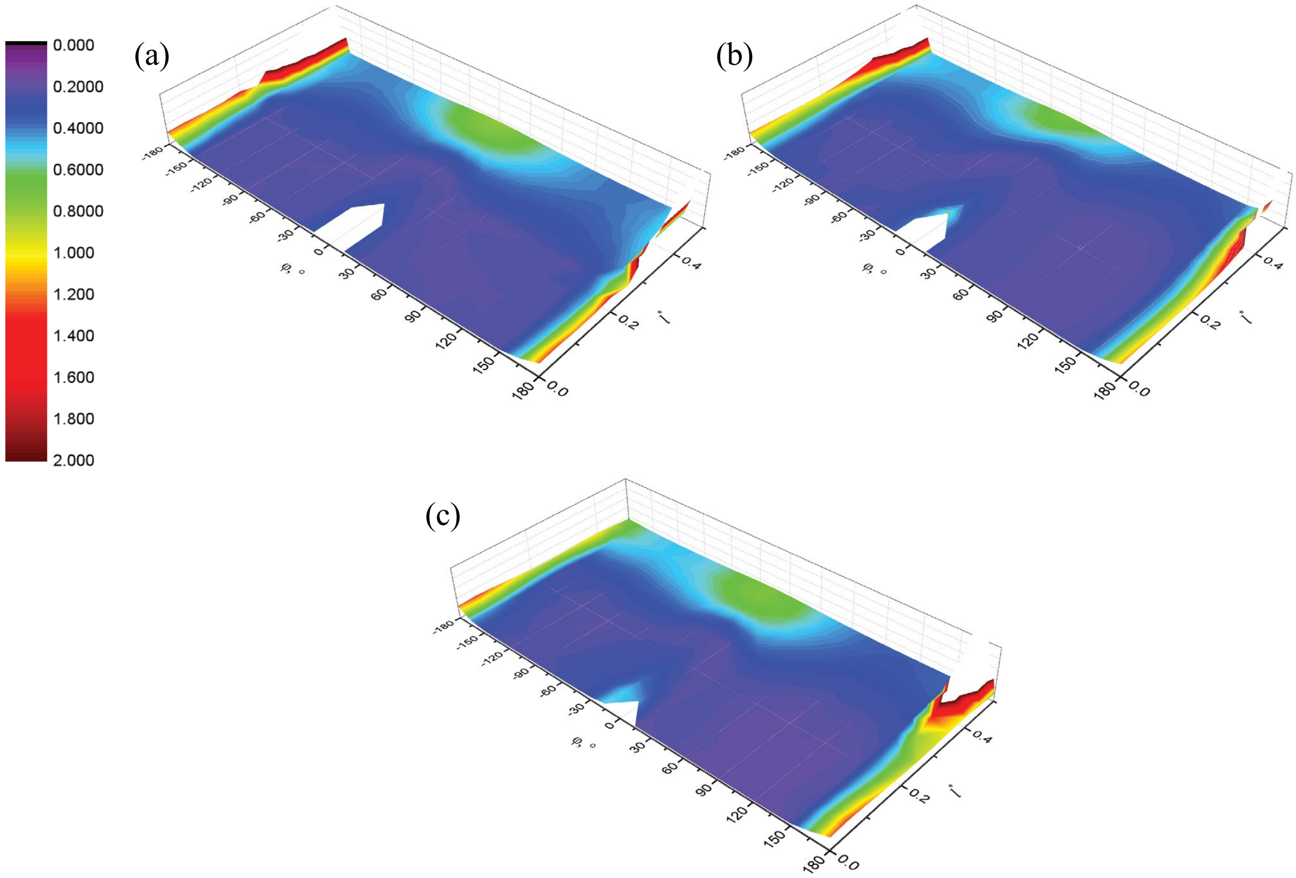

Fig. 7. Three-dimensional film thickness distribution with gas crossflow velocity. (a) u = 0.2 m/s, (b) u = 0.6 m/s, and (c) u = 1.0 m/s.

decreases. The streamline images of single phase shown in Fig. 8 help us to understand the film distribution.

3.2.2. Effect of Reynolds number

Figs. 9a–c show the variations with spray Reynolds number. The reduction in spray Reynolds number results in decreasing of spray density, which thins liquid column between tubes and film around the tube. According to the analysis of liquid column deflection, the liquid column with small Re is more sensitive to be influenced by the crossflow. At l^* = 0, the film at leeward from –150° to –30° is little affected by the variation of Re, but in windward, an obvious decline can be observed in the range of 90°–150°. The film thickness of l^* = 0.25, wherever at leeward or windward, is generally stabilized in 0.2–0.25 mm except in the bottom region. Fig. 9c clearly shows the "crest" at l^* = 0.5 moves to windward when the Re increases.

Three-dimensional film thickness morphologies in Figs. 10a–c show that the departure liquid column gradually moves to windward with decreasing of Re. With the same crossflow velocity, the smaller Re leads to the thinner film in the stable region especially ϕ > 90°. It also can be found that the thinnest film appears at 75°–150° with l^* = 0–0.2, it decreases to the value that smaller than 0.18 mm under the condition of u = 0.6 m/s and Re = 221.

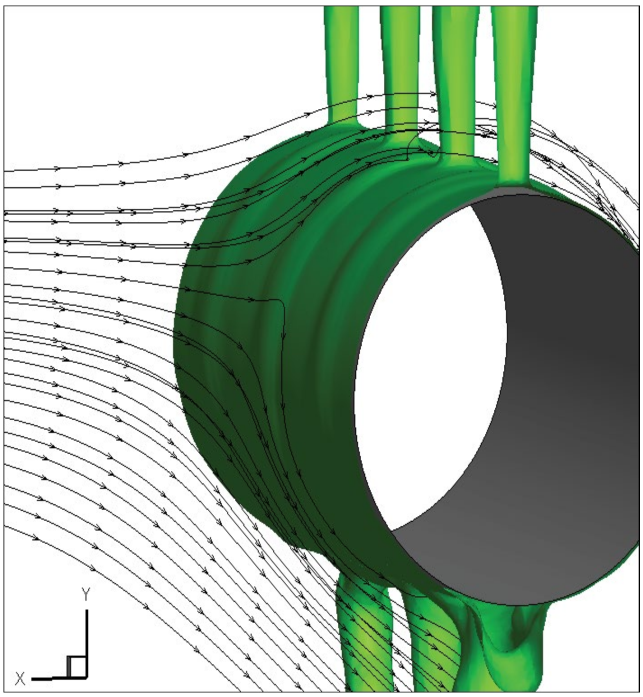

Fig. 8. Streamlines of gas crossflow.

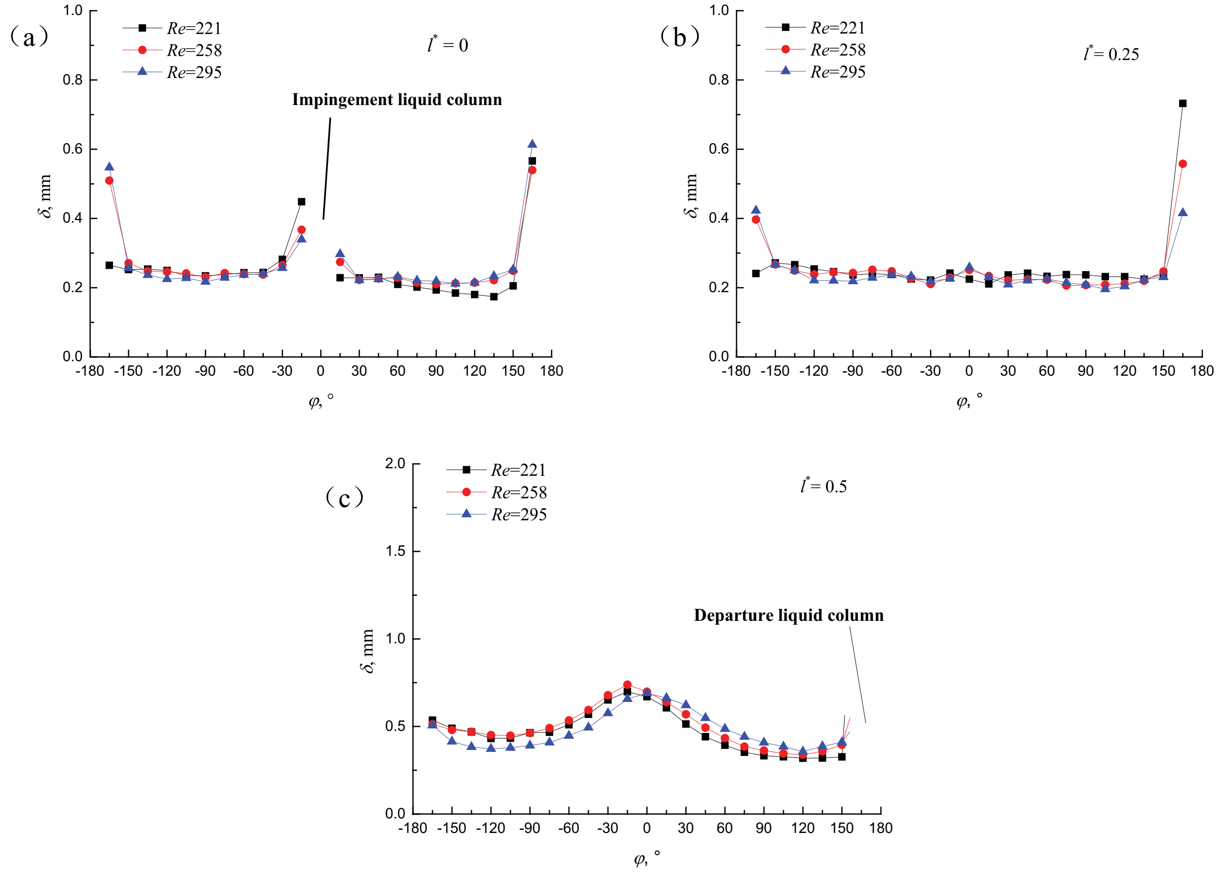

Fig. 9. Effect of Re on film thickness. (a) l^* = 0, (b) l^* = 0.25, and (c) l^* = 0.5.

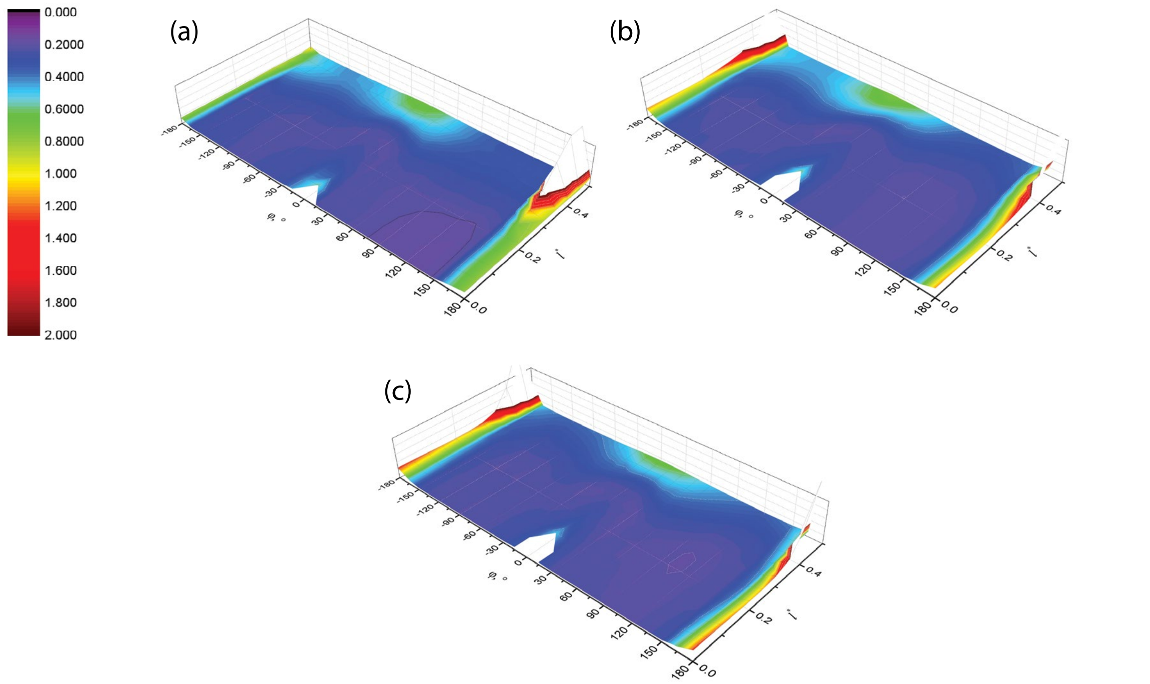

Fig. 10. Film thickness distribution with Reynolds number. (a) u = 0.6 m/s, Re = 221, (b) u = 0.6 m/s, Re = 258, and (c) u = 0.6 m/s, Re = 295.

Compared with the film distributions in quiescent surroundings [22], the crossflow depresses the positive effect on film thickness from the Re increasing due to the film acceleration resulted from gas crossflow shear force.

4. Conclusions

A three-dimensional numerical simulation was conducted to study the horizontal tube falling film flow with gas crossflow, the conclusions are shown as follows:

- The liquid column deflection angle increases with crossflow velocity and decreases with spray Reynolds number. Simultaneously, the crest also moves toward leeward. Moreover, the departure liquid column deflects to windward.
- Crossflow results in the misdistribution along leeward and windward, especially the liquid film at the impingement and departure section. It lowers the film thickness at the windward and enhances the film thickness at leeward as the crossflow velocity increasing. The thinnest film appears at l^* = 0–0.2, ϕ = 75°–150° in the "stable region" of windward. With the crossflow velocity increases, the film thickness in the stable region of windward decreases.
- Compared with the film thickness distribution in quiescent surroundings, the crossflow depresses the positive effect on film thickness from the Re increasing.

Acknowledgment

The authors acknowledge the support from National Natural Science Foundation of China (No. 51706011, No. 51776014) and China Postdoctoral Science Foundation (No. 2018M641163).

Symbols

d — Tube diameter, mm
d_c^* — Equivalent diameter of liquid column, mm
F_d — Drag force, N
G — Gravity, N
g — Gravitational acceleration, m/s^2
h_w — Height from upper tube to inlet, mm
h_l — Height from model bottom to lower tube, mm
Re — Spray Reynolds number, $4\Gamma/\mu$
l — Length, mm
l^* — Non-dimensional axial length in a fluid unit
s — Tube spacing, mm
t — Time, s
w — Inlet width, mm
u — Crossflow velocity, m/s

Greek

α_q — Phase volume fraction
β_c — Deflection angle of liquid column, °
β_p — Deflection angle of departure point, °
σ — Surface tension, N/m
δ — Film thickness, mm
ϕ — Circumferential angle, °
μ — Dynamic viscosity, kg/(m s)
θ — Contact angle, °
ρ — Density, kg/m^3
Γ — Spray density per side, kg/(m s)
λ — Distance between two adjacent columns (departure-site spacing), mm

Subscripts

x, y, z — Cartesian coordinate system

References

[1] G. Ribatski, A.M. Jacobi, Falling-film evaporation on horizontal tubes-a critical review, Int. J. Refrig., 28 (2005) 635–653.
[2] M.E. Alvarez, M. Bourouis, Experimental characterization of heat and mass transfer in a horizontal tube falling film absorber using aqueous (lithium, potassium, sodium) nitrate solution as a working pair, Energy, 148 (2018) 876–887.
[3] L.Y. Gong, S.Q. Shen, H. Liu, X.S. Mu, X. Chen, Three-dimensional heat transfer coefficient distributions in a large horizontal-tube falling film evaporator, Desalination, 357 (2015) 104–116.
[4] J. Fernández-Seara, Á.Á. Pardiñas, Refrigerant falling film evaporation review: description, fluid dynamics and heat transfer, Appl. Therm. Eng., 64 (2014) 155–171.
[5] L. Xu, M.R. Ge, S.C. Wang, Y.X. Wang, Heat transfer film coefficients of falling film horizontal tube evaporators, Desalination, 166 (2004) 223–230.
[6] S.Q. Shen, X. Chen, X.S. Mu, Y.X. Wang, L.Y. Gong, Heat transfer characteristics of horizontal tube falling film evaporation for desalination, Desal. Water Treat., 55 (2015) 3343–3349.
[7] A. Raju, A. Mani, Heat transfer characteristics in horizontal tube bundles for falling film evaporation in multi-effect desalination system, Desalination, 375 (2015) 129–137.
[8] C.Y. Zhao, W.T. Ji, Y.L. He, Y.J. Zhong, W.Q. Tao, A comprehensive numerical study on the subcooled falling film heat transfer on a horizontal smooth tube, Int. J. Heat Mass Transfer, 119 (2018) 259–270.
[9] L. Xu, S.C. Wang, Y.X. Wang, Y. Ling, Flowing state in liquid films over horizontal tubes, Desalination, 156 (2003) 101–107.
[10] T.J. Rogers, S.S. Goindi, Experimental laminar falling film heat transfer coefficients on a large diameter horizontal tube, Can. J. Chem. Eng., 67 (1989) 560–568.
[11] B. Narváez-Romo, J.R. Simões-Moreira, Falling liquid film Evaporation in subcooled and saturated water over horizontal heated tubes, Heat Transfer Eng., 38 (2017) 361–376.
[12] H. Hou, Q.C. Bi, H. Ma, G. Wu, Distribution characteristics of falling film thickness around a horizontal tube, Desalination, 285 (2012) 393–398.
[13] D. Gstoehl, J.F. Roques, P. Crisinel, J.R. Thome, Measurement of falling film thickness around a horizontal tube using a laser measurement technique, Heat Transfer Eng., 25 (2004) 28–34.
[14] X. Chen, S.Q. Shen, Y.X. Wang, J.X. Chen, J.S. Zhang, Measurement on thickness distribution of falling film around horizontal tube with laser-induced fluorescence technology, Int. J. Heat Mass Transfer, 89 (2015) 707–713.
[15] L.C. Luo, G.M. Zhang, J.H. Pan, M.C. Tian, Flow and heat transfer characteristics of falling water film on horizontal circular and non-circular cylinders, J. Hydrodyn., 25 (2013) 404–414.
[16] C.Y. Zhao, W.T. Ji, P.H. Jin, Y.J. Zhong, W.Q. Tao, Hydrodynamic behaviors of the falling film flow on a horizontal tube and construction of new film thickness correlation, Int. J. Heat Mass Transfer, 119 (2018) 564–576.
[17] G. Ji, J.F. Wu, Y.P. Chen, G.J. Ji, Asymmetric distribution of falling film solution flowing on hydrophilic horizontal round tube, Int. J. Refrig., 78 (2017) 83–92.
[18] J.D. Killion, S. Garimella, Simulation of pendant droplets and falling films in horizontal tube absorbers, J. Heat Transfer, 126 (2004) 1003–1013.

[19] Y.H. Zhou, Z. Cai, Z. Ning, M.S. Bi, Numerical simulation of double-phase coupled heat transfer process of horizontal-tube falling film evaporation, Appl. Therm. Eng., 118 (2017) 33–40.
[20] M.J. Li, Y. Lu, S.J. Zhang, Y.H. Xiao, A numerical study of effects of counter-current gas flow rate on local hydrodynamic characteristics of falling films over horizontal tubes, Desalination, 383 (2016) 68–80.
[21] S.M. Hosseinnia, M. Naghashzadegan, R. Kouhikamali, CFD simulation of water vapor absorption in laminar falling film solution of water-LiBr — drop and jet modes, Appl. Therm. Eng., 115 (2017) 860–873.
[22] J. Wang, X. Chen, T. Lu, X.S. Chen, S.Q. Shen, B. Liu, Three-dimensional film thickness distribution of horizontal tube falling film with column flow, Appl. Therm. Eng., 154 (2019) 140–149.
[23] L.Y. Gong, S.Q. Shen, H. Liu, X.S. Mu, Parametric distributions of a horizontal-tube falling film evaporator for desalination, Desal. Water Treat., 57 (2015) 11699–12117.
[24] C. Yao Zhao, W.T. Ji, P.H. Jin, W.Q. Tao, Cross vapor stream effect on falling film evaporation in horizontal tube bundle using R134a, Heat Transfer Eng., 39 (2018) 724–737.
[25] C.Y. Zhao, W.T. Ji, P.H. Jin, S. Yoshioka, W.Q. Tao, Effect of downward vapor stream on falling film evaporation of R134a in a tube bundle, Int. J. Refrig., 89 (2018) 112–121.
[26] D. Yung, J.J. Lorenz, E.N. Ganić, Vapor/liquid interaction and entrapment in falling film evaporators, J. Heat Transfer, 102 (1980) 20–25.
[27] X. Hu, A.M. Jacobi, The intertube falling film. Part 1. Flow characteristics, mode transitions, and hysteresis, J. Heat Transfer, 118 (1996) 616–6525.
[28] X.L. Lei, H.X. Li, L.B. Yan, B. Guo, Numerical investigation on the offset characteristics of falling liquid columns over horizontal tubes under the interaction of inter-tube gas flows, J. Eng. Thermphys., 31 (2010) 1875–1878 (in Chinese).
[29] B.L. Ruan, A.M. Jacobi, L.S. Li, Effects of a countercurrent gas flow on falling-film mode transitions between horizontal tubes, Exp. Therm. Fluid Sci., 33 (2009) 1216–1225.
[30] J.G. Bustamante, S. Garimella, Experimental assessment of flow distributors for falling-films over horizontal tube banks, Int. J. Refrig., 101 (2019) 24–33.
[31] Ansys Incorporated, Ansys Fluent 16.0 Theory Guide, USA, 2015.